Lytic versus stimulatory synapse in cytotoxic T lymphocyte/target cell interaction: Manifestation of a dual activation threshold

Mustapha Faroudi*†, Clemens Utzny*†, Mariolina Salio‡, Vincenzo Cerundolo‡, Martine Guiraud*, Sabina Müller*, and Salvatore Valitutti*§

*Lymphocyte Interaction Group, Institut Claude de Préval, Institut National de la Santé et de la Recherche Médicale U563, 31059 Toulouse, France; and ‡Cancer Research UK, Tumor Immunology Group, John Radcliffe Hospital, Oxford OX3 9DS, United Kingdom

Edited by Herman N. Eisen, Massachusetts Institute of Technology, Cambridge, MA, and approved September 24, 2003 (received for review July 11, 2003)

Activation of biological functions in T lymphocytes is determined by the molecular dynamics occurring at the T cell/opposing cell interface. In the present study, a central question of cytotoxic T lymphocyte (CTL) biology was studied at the single-cell level: can two distinct activation thresholds for cytotoxicity and cytokine production be explained by intercellular molecular dynamics between CTLs and targets? In this study, we combine morphological approaches with numerical analysis, which allows us to associate specific patterns of calcium mobilization with different biological responses. We show that CTLs selectively activated to cytotoxicity lack a mature immunological synapse while exhibiting a low threshold polarized secretion of lytic granules and spike-like patterns of calcium mobilization. This finding is contrasted by fully activated CTLs, which exhibit a mature immunological synapse and smooth and sustained calcium mobilization. Our results indicate that intercellular molecular dynamics and signaling characteristics allow the definition of two activation thresholds in individual CTLs: one for polarized granule secretion (lytic synapse formation) and the other for cytokine production (stimulatory synapse formation).

The interaction between cytotoxic T lymphocytes (CTLs) and target cells begins with the random conjugate formation mediated by adhesion molecules. Subsequent recognition of specific antigen results in the activation of signal transduction pathways coupled to T cell antigen receptors (TCRs) and accessory molecules. This process leads to the effector phase consisting of perforin-mediated and/or Fas ligand-mediated delivery of the lethal hit (1, 2). Killing can be triggered by as few as 1–10 specific peptide–MHC complexes displayed on the target cell and requires a short time (3); consequently, killer cells form sequential conjugates and kill multiple targets (4, 5).

An intriguing feature of CTL biology is that cytotoxicity and full activation are uncoupled. Activation of biological CTL responses such as IL production and proliferation requires a prolonged time and is achieved only with an adequate antigenic stimulation (6, 7).

The resulting dose–response curves in CTL activation are well established on the population level by using methods that measure target cell death together with IL release by CTLs (6, 7). However, these approaches have never addressed the question of how individual CTLs may exhibit two distinct activation thresholds: one for target elimination, the other for clonal expansion.

Another unresolved question concerns the functional relation between the cytotoxic response and the immunological synapse (IS). In its original definition, the mature IS was described as a specialized signaling domain formed at the contact site between T cells and antigen-presenting cells (APCs), characterized by large-scale molecular segregation of surface receptors and signaling components (8–10). Current research leads to an expansion of this term, where the IS comprises a multitude of structures, all of them having in common that they are mediators of intercellular communication (11).

The role of the IS is still elusive, and it may serve several not mutually exclusive functions. The IS could either augment and sustain signal transduction at the beginning of T cell activation (12) or extinguish it by accelerating TCR down-regulation (13).

In CTLs the IS may have the role of favoring polarized secretion of lytic granules toward target cells (10). However, because the formation of a mature IS requires several minutes (13), it is unlikely that it plays a role in initiating cytotoxic function (10). This raises the question about the role of the mature IS in cytotoxicity.

To address the above questions, signaling aspects were studied in parallel with functional responses in individual CTLs.

We used confocal microscopy and fluorescence-activated cell sorting (FACS) analysis to document morphological parameters of CTL activation. We show that polarized secretion of perforin toward target cells is achieved in individual CTLs at antigen concentrations sufficient to elicit cytotoxicity (lytic synapse). We also demonstrate that this occurs in the absence of the molecular rearrangement characteristic for the mature IS (stimulatory synapse).

Second, the intracellular Ca^{2+} concentration ($[Ca^{2+}]_i$) mobilization in activated CTLs was measured to probe intracellular signaling. Calcium mobilization is known to play a central role in the activation of biological functions in T lymphocytes (14–17). Also, in CTLs lytic granule exocytosis requires calcium influx (18–20), whereas reorientation of the microtubule organizing center toward the target cell is calcium-dependent (21).

We measured $[Ca^{2+}]_i$ in antigen-stimulated individual CTLs. Using a numerical analysis of calcium mobilization we detect significant differences in the $[Ca^{2+}]_i$ pattern in the different experimental conditions. We find that at low peptide concentration (sufficient for cytotoxicity) the $[Ca^{2+}]_i$ patterns show more pronounced spikes of calcium mobilization as compared with high peptide concentration. This finding indicates that in CTLs the quality of calcium response changes according to the strength of TCR stimulation.

All in all, our results show two activation thresholds in individual CTLs that are characterized by synapse structure and signaling patterns.

Experimental Procedures

T Cells and APCs. An HLA-A2-restricted T cell line, CMVpp65, specific for the human cytomegalovirus protein peptide

This paper was submitted directly (Track II) to the PNAS office.

Abbreviations: CTL, cytotoxic T lymphocyte; TCR, T cell antigen receptor; IS, immunological synapse; APC, antigen-presenting cell; FACS, fluorescence-activated cell sorting; $[Ca^{2+}]_i$, intracellular Ca^{2+} concentration; EBV, Epstein–Barr virus; LTR, LysoTracker red.

See Commentary on page 13739.

†M.F. and C.U. contributed equally to this work.

§To whom correspondence should be addressed. E-mail: svalitu@toulouse.inserm.fr.

pp65 (NLVPMVATV) was used. Spectratyping analysis of the TCR repertoire (22) revealed that this is a polyclonal line expressing the following Vβ families: 3, 5, 6, 8, 13, 14, 16, 18, 21, and 23 (data not shown). HLA-A2 matched Epstein–Barr virus (EBV)-transformed B cells were used as target cells. T cell line and EBV-B cell lines were generated and maintained as described (15).

Cytolytic Activity Assay. Standard 4-h ^{51}Cr release assays were used to assess antigen-specific target cell lysis as described (6).

IFN-γ Production and TCR Down-Regulation. IFN-γ production and TCR down-regulation were measured by FACS analysis in CTL-target conjugates 4 h after conjugate formation as described (6).

Intracellular Staining. T cells were conjugated with EBV-B cells previously loaded with 0.5 μM Orange-CMTMR (Molecular Probes) either unpulsed or pulsed with the specific peptide as described (23). After washing, T cells were mixed with EBV-B cells at a 1:1 ratio in 200 μl of RPMI medium 1640/5% FCS in U-bottom tubes and centrifuged to allow conjugate formation. After 10 min at 37°C, the cells were gently resuspended and laid on poly-L-lysine coated slides for 3 min at 37°C. The cells were fixed for 10 min at room temperature with 3% paraformaldehyde, permeabilized for 10 min with Hepes-buffered PBS containing 0.1% saponin, 3% BSA (23), and stained with antiphosphotyrosine mAbs (Santa Cruz Biotechnology), anti-CD2 (Pharmingen), anti-human perforin mAb (Pharmingen), and antitubulin mAbs (Sigma), followed by isotype-matched, Cy5-labeled goat anti-mouse Abs (Caltag Laboratories, Burlingame, CA) and FITC-labeled goat anti-mouse Abs (Southern Biotechnology Associates) as described (23). In some experiments, T cells were pretreated for 30 min before conjugation with LysoTracker red (LTR) (Molecular Probes). The samples were mounted and examined by using a Carl Zeiss LSM 510 confocal microscope with a $\times$63 Plan-Apochromat objective (1.4 oil). An argon laser at 488 nm was used to detect fluorescein fluorochrome. To detect Orange-CMTMR fluorescence a helium-neon laser was filtered at 543 nm. To detect Cy5 fluorescence a helium-neon laser was filtered at 633 nm. Under standard imaging conditions no signal from one fluorochrome could be detected with the other filter set. For each pair of antibodies used, standardized conditions for pinhole size and for gain and offset were used for image capture.

Measurement of Intracellular Perforin by FACS Analysis. CTLs and target cells were conjugated at the 1:2 ratio as described above. After 2 h culture cells were washed in ice-cold PBS containing 0.5 mM EDTA, fixed permeabilized (as described above), and stained with antiperforin antibodies followed by isotype-matched, FITC-labeled goat anti-mouse Abs. The perforin fluorescence was analyzed on a FACScan. EBV-B cells were gated out by using both forward light scatter/sidelight scatter parameters and red Orange-CMTMR fluorescence.

Fluorescence Imaging and [Ca^{2+}] Analysis. T cells were incubated with 5 μM Fura 2-AM (Molecular Probes) for 45 min at 37°C in 5% FCS Hepes-buffered RPMI medium 1640. After washing, Fura-2-loaded T cells were dropped onto target cells previously pulsed with various concentrations of the specific peptide and attached to a poly-L-lysine-coated slide to form a monolayer. The existence of a target cell monolayer was checked at the beginning and end of the recording time by visualizing the cells with transmitted light. Fluorescence measurements were done on a Zeiss axiovert 200M inverted microscope equipped with a charge-coupled device (CCD) camera (Princeton Instruments, Trenton, NJ), an arc-xenon lamp, and a computer-controlled monochromator (TILL Photonics, Planegg, Germany) at 37°C, 5% CO_2. Cells were consecutively excited with 340 and 380 nm at 5-s intervals by means of the monochromator, and both emissions were collected with the CCD camera. The total acquisition time was 45 min. The camera output was analyzed by using custom calcium-imaging software, METAFLUOR, provided by Universal Imaging (West Chester, PA). The Fura 2-loaded CTLs changed the ratio of excitation at 340 and 380 nm upon $[Ca^{2+}]_i$ rise. The emission intensity at any time point was ratioed, and the results were displayed on a pseudocolor scale. Calculation of the ratios was done by the software on randomly selected cells.

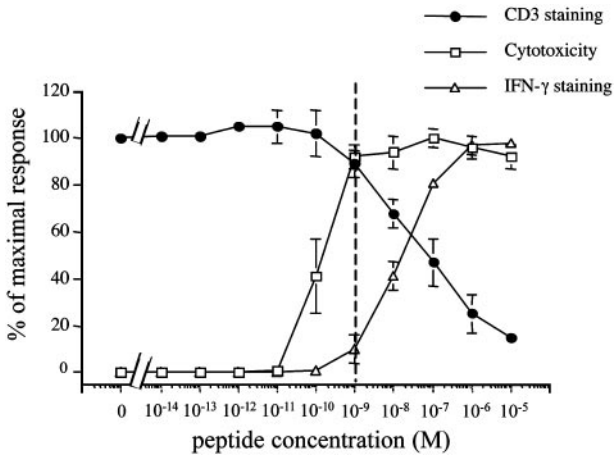

Fig. 1. IFN-γ production and TCR down-regulation require a higher antigen concentration than cytotoxicity. CTLs were conjugated with target cells in the presence of different concentrations of pp65. Cytotoxicity (□), IFN-γ production (△), and CD3 down-regulation (●) were measured after 4 h at 37°C. The effector-to-target cell ratio (E/T ratio) was 2:1 in the presented experiments. Similar results were obtained by using other E/T ratios (6:1, 0.6:1, 0.2:1). Data are from three independent experiments performed in duplicate for each assay. Results are expressed as means ± SD of the three experiments.

[Ca^{2+}]$_i$ Data Analysis. The statistical analysis of the $[Ca^{2+}]_i$ data was performed by using the TISEAN 2.1 (24) and R software packages. Detrending of the time series was done by using robust locally linear fits as implemented in the "loess" algorithm of R with the default window size, i.e., two-thirds of the data are included for each local fit. However, the results are robust with respect to changes of the window size and use of different smoothing algorithms. The temporal evolution of the mean spikiness has been computed by using averaging windows of size 5, 10, 30, and 60 s, all giving similar results. The 95% confidence intervals and statistical significance for the data (see Fig. 5) was tested by using the parameter-free Wilcoxon test as implemented in R.

Results

Different Activation Thresholds for Cytotoxicity and IL Production. Initially, we investigated the ranges of antigen concentrations that induce cytotoxicity and/or other biological functions at the population level.

TCR down-regulation and IFN-γ production were measured by FACS analysis in human CTL–target cell conjugates. In parallel experiments cytotoxicity was investigated by measuring ^{51}Cr release from target cells.

In agreement with previously reported data (6, 7), we found that CTLs exhibit cytotoxicity at antigen concentrations at which other responses are either undetectable or very low. Fig. 1 shows that cytotoxicity is saturated at peptide concentrations of 1 nM. At this antigen concentration only $\approx$10% of the maximal TCR

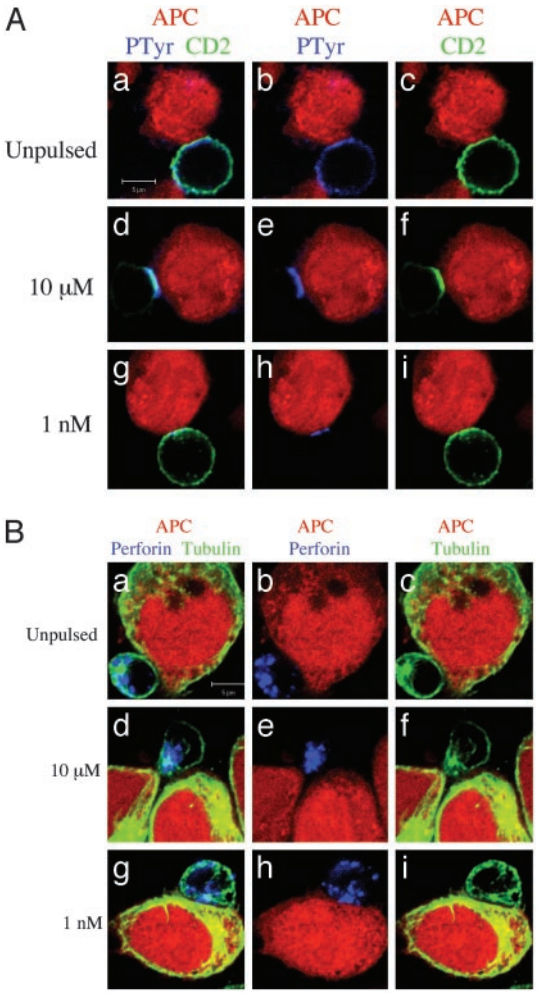

Fig. 2. IS formation is not required for CTL polarization toward target cells. CTLs were conjugated with EBV-B cells (red). After 10 min at 37°C cells were stained with the following antibodies. (*A*) Antiphosphotyrosine mAb (blue) and anti-CD2 mAb (green). (*B*) Antiperforin mAb (blue) and antitubulin mAb (green). APCs were either unpulsed (*a–c*) or pulsed with either 10 μM (*d–f*) or 1 nM (*g–i*) pp65. *a*, *d*, and *g* are three-color images. In *b*, *e*, and *h* the green color has been removed. In *c*, *f*, and *i* the blue color has been removed. Data are from one representative experiment of six. (Bars = 5 μM.)

down-regulation and IFN-γ production were observed. Conversely, both TCR down-regulation and IFN-γ production were maximal at the concentrations of 10 μM.

Therefore, we chose the above antigen concentrations (1 nM and 10 μM) to study different activation parameters of individual CTLs interacting with their target cells.

Lytic Versus Stimulatory Synapse in CTL–Target Cell Conjugates. Using confocal microscopy, we have demonstrated the rapid formation of a signaling domain at the contact site between T helper cells and APCs characterized by a broad and sustained area of tyrosine phosphorylation and by the recruitment of CD2 (23).

Hence, we used these markers as a parameter for the formation of a stimulatory IS in individual CTLs. At 10-μM antigen concentration, a broad area of phosphorylation and accumulation of CD2 at the CTL–target contact area were observed in most conjugates, indicating that also in CTLs this phenotype correlates with full activation (Fig. 2*A d–f* and Table 1). Conversely, at 1-nM antigen concentration, this molecular reorganization was less pronounced and present in only a small fraction of conjugates (see Fig. 2*A g–i* in which a typical moderate enrichment of CD2 and phosphotyrosine is depicted and Table 1). In addition, it should be noted that a small fraction of conjugates formed between CTLs and unpulsed target cells also exhibited a modest enrichment of phospotyrosine and CD2 at the cellular interface (Fig. 2*A a–c* and Table 1). Therefore, only small differences between the two phenotypes, no antigen versus 1-nM antigen concentration, were detectable (Fig. 2 and Table 1).

Table 1. Measurement of the distribution of phosphotyrosines, CD2, tubulin, and perforin at the CTL-target contact site

	No peptide		10 μM		1 nM	
Enrichment	%	*n*	%	*n*	%	*n*
Phosphotyrosine		121		119		117
No	81		6		65	
Weak	19		0		32	
Strong	0		94		3	
CD2	16	118	85	139	25	140
Tubulin and perforin	14	146	74	145	68	155

For each antibody *n* CTL-target conjugates were randomly selected from three independent experiments and scored for CD2 and phosphotyrosine enrichment and tubulin cytoskeleton and perforin polarization at the cell–cell contact site. Segregation was scored by visual inspection in a double-blind study. Tubulin and perforin were scored together, and only CTLs exhibiting polarization of both tubulin and perforin were scored as positive. *n*: number of conjugates analyzed. %: percent of conjugates exhibiting a given pattern of staining for *n* = 100%.

For CD2 staining an enrichment corresponded to a 1.5-fold fluorescence increase at the contact region versus the rest of the cell. For phosphotyrosine staining strong weak and no signaling activity were scored by visual inspection only in a double-blind study.

In parallel experiments we studied the morphological parameters of lethal hit delivery. We focused on lytic granule exocytosis as it represents the major molecular mechanism for CTL cytotoxicity (25). CTL/target cell conjugates were fixed, permeabilized, and stained with anti-β-tubulin and antiperforin antibodies to visualize the polarization of the lytic machinery toward the target cells by confocal microscopy. As shown in Fig. 2*B a–c* and Table 1, CTLs interacting with unpulsed target cells did not polarize tubulin cytoskeleton nor perforin granules toward the opposing cells.

Strikingly, the majority of the CTLs interacting with target cells pulsed with 1-nM antigen concentration exhibited polarization of tubulin cytoskeleton and perforin granules toward the target cells (Fig. 2*B g–i* and Table 1). It should be noted that in some conjugates granule enrichment at the contact site was incomplete while the microtubule organizing center was pointing toward the target (Fig. 2*Bh*). This result is in agreement with previously reported data showing that cellular polarization precedes the orientation of perforin granules toward the target cells (10).

Finally, at antigen concentrations of 10 μM the fraction of CTLs polarized toward target cells was as large as for concentrations of 1 nM (see Table 1); however, in these conditions, most of the perforin granules were accumulated at the cellular interface (Fig. 2*B d–f*).

To improve the characterization of lethal hit delivery by CTLs, we exploited the fact that lytic granules of CTLs are secretory lysosomes (26, 27) that can be labeled *in vivo* by using LTR. CTLs were therefore loaded with LTR before conjugation with target cells. After fixation and permeabilization, the cells were stained with antiperforin antibodies and either anti-CD2 or antitubulin antibodies. As shown in Fig. 3, this approach confirmed that at 1-nM antigen concentration the lytic machinery is oriented

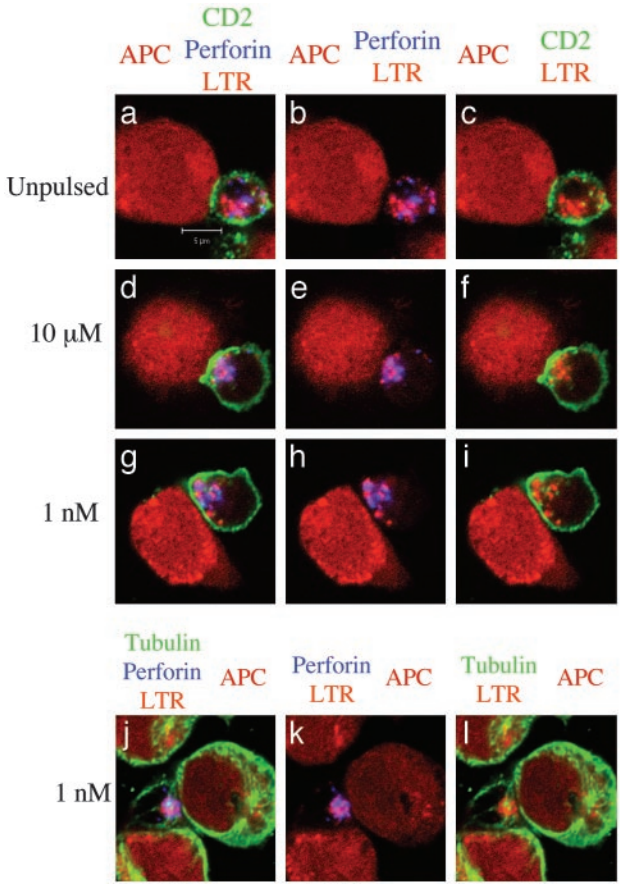

Fig. 3. Reorientation of CTL lytic machinery in the absence of CD2 enrichment at the cell–cell contact site. T cells were pretreated with LTR before conjugation with target cells unpulsed (*a–c*) or pulsed with either 10 μM (*d–f*) or 1 nM (*g–l*) pp65. After 10 min at 37°C cells were stained with either anti-CD2 mAbs (green) and antiperforin mAbs (blue) (*a–i*) or antitubulin mAbs (green) and anti-perforin mAbs (blue) (*j–l*). *a*, *d*, *g*, and *j* are three-color images. In *b*, *e*, *h*, and *k* the green color has been removed. In *c*, *f*, *i*, and *l* the blue color has been removed. Data are from one representative experiment of three. (Bar = 5 μM.)

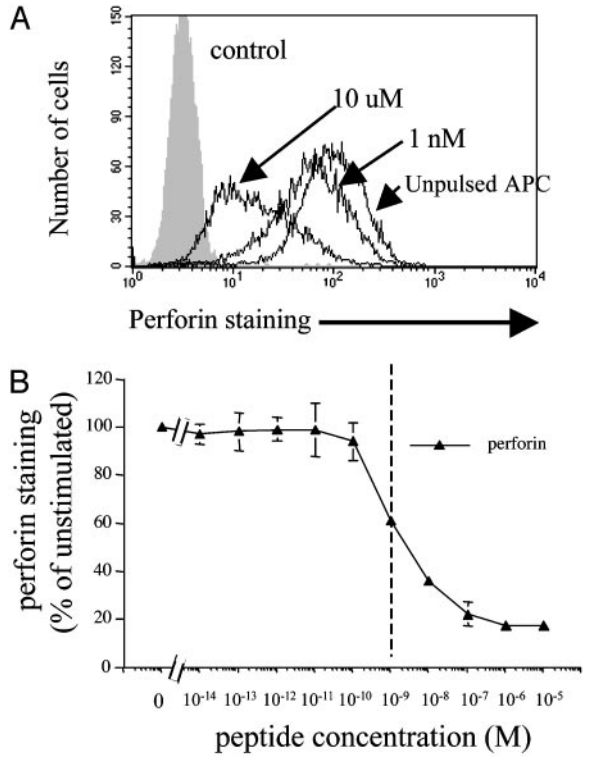

Fig. 4. Antigen dose-dependent decrease of perforin intracellular content in CTLs. (*A*) Staining for perforin in CTLs that have been conjugated for 2 h with EBV-B cell unpulsed or pulsed with either 10 μM or 1 nM pp65. (*B*) Levels of perforin staining as a function of antigen concentration. Data are from three independent experiments performed in duplicate. Results are expressed as means ± SD of the three experiments.

toward target cells in the absence of CD2 accumulation at the cellular interface.

As a whole, the above results demonstrate that the polarization of the lytic machinery toward the target cell is already saturated in individual CTLs at the low antigen concentration that is not sufficient to elicit the molecular segregation characteristic of a mature IS. Thus, they suggest that a low threshold signaling mechanism selectively induces the formation of a lytic synapse at the CTL/target contact site.

Perforin Secretion by Individual CTLs Has a Low Activation Threshold. To improve the understanding of the activation of cytotoxic function in individual CTLs we investigated the possibility of measuring a parameter correlated with lethal hit delivery by FACS analysis.

Therefore, perforin content was measured by FACS analysis in fixed and permebilized CTL–target conjugates. This analysis revealed an antigen dose-dependent loss of perforin in CTLs (Fig. 4). Interestingly, at the 1-nM concentration, perforin staining was decreased by ≈40%, whereas the response was maximal at the 100-nM concentration (Fig. 4*B*). The observation that at concentrations of 1 nM perforin staining was decreased by ≈40% is consistent with our morphological data showing that at this antigen concentration most CTLs have already polarized their tubulin cytoskeleton, while some perforin granules are still dispersed throughout the cytosol (Fig. 2*Bh*). Also, perforin loss was consistently observed in the entire CTL population (Fig. 4*A*). indicating that, at low antigen concentration, nearly all CTLs in the population exhibit cytotoxicity.

These results indicate that individual CTLs exhibit a low activation threshold to initiate perforin release.

Spiky Signaling Correlates with the Existence of a Rudimentary Synapse. As a next step in the characterization of signaling, we measured $[Ca^{2+}]_i$ in CTLs interacting with target cells either unpulsed or pulsed with two peptide concentrations (10 μM, sufficient for full CTL activation; 1 nM, where only cytotoxicity is saturated). The beginning of significant signaling was defined by an unambiguous elevation of $[Ca^{2+}]_i$ above the basal level; the first 10 min of calcium mobilization after this elevation were used for the quantitative analysis of 113 calcium patterns (31 for unpulsed targets, 38 for peptide concentration of 1 nM, and 44 for peptide concentration of 10 μM).

CTLs interacting with unpulsed targets exhibited diverse patterns of calcium mobilization. Some cells exhibited a single calcium spike followed by a return to the basal level for a prolonged time; other cells were undergoing a sustained but moderate calcium mobilization. Finally, a significant fraction of the CTLs in contact with the monolayer of unpulsed targets exhibited no $[Ca^{2+}]_i$ mobilization (data not shown). Thus the beginning of significant signaling cannot be defined unambiguously in these cells; therefore, the no pulse data were excluded from the statistical analysis.

Fig. 5 *A* and *B* depicts typical $[Ca^{2+}]_i$ patterns obtained for the two peptide concentrations. $[Ca^{2+}]_i$ at concentrations of 10 μM

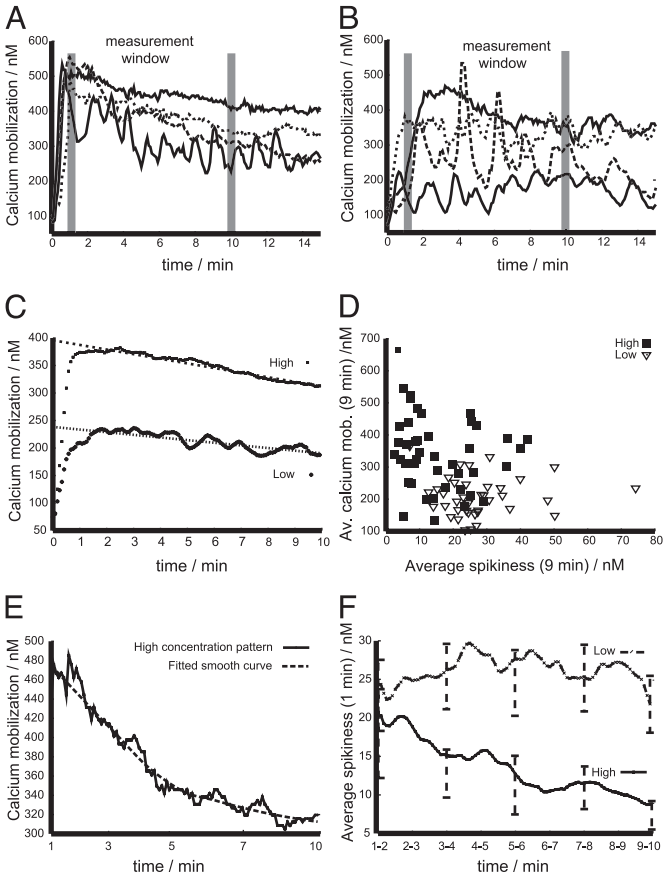

Fig. 5. Spiky signaling in CTLs stimulated with low antigen concentration. (*A* and *B*) Typical calcium mobilization patterns are depicted: high concentration patterns (*A*) and low concentration patterns (*B*). (*C*) The ensemble average of the calcium flux over time is shown. (*D*) The correlation of spikiness and mean calcium flux is shown. (*E*) An examplatory fitting of a smooth curve to a time series is given. (*F*) The temporal evolution of the ensemble average of the signal pattern spikiness is depicted for both specific peptide concentrations.

mount to high levels and are sustained for a prolonged time (Fig. 5*A*); for antigen concentrations of 1 nM the patterns are more irregular and mount to lower levels but can be sustained for long times as well (Fig. 5*B*); however, in both cases the $[Ca^{2+}]_i$ patterns exhibit a pronounced diversity in their structure.

In Fig. 5*C* the ensemble mean (i.e., the average of all 44 and 38 time series) of the two sets of calcium patterns is depicted. Both curves demonstrate that under the two experimental conditions a significant difference in the total amount of calcium mobilization was observed. Furthermore, both sets of data exhibited a signal saturation after 1 min of signaling together with an approximately linear signal decline over the next 9 min.

The patterns presented in Fig. 5 *A* and *B* suggest that besides the signaling level the general shape of the $[Ca^{2+}]_i$ time series differs for the two peptide concentrations. In Fig. 5*D* a scatter plot of average calcium mobilization versus the average spikiness is presented. The spikiness of each signal is computed by fitting a smooth line to each time series (Fig. 5*E*). The distance (root of the mean squared) between the data and the curve is the spikiness (to exclude influences from the basal level both averages are taken over the first 9 min after the mean signal is saturated, i.e., leaving the first minute of $[Ca^{2+}]_i$ out). The scatter plot demonstrates the tendency of high concentration patterns to be smooth (small spikiness), which is in contrast to low concentration patterns that tend to have a lower average calcium mobilization but a higher spikiness (Fig. 5*D*).

To follow the temporal evolution of spikiness the ensemble average of the spikiness evaluated over a measurement window of 1-min length was computed, and the measurement window was moved through the first 9 min of the saturated signaling (Fig. 5*F*, the bars computed every 2 min give the 95% confidence interval). It follows that the average spikiness of the two sets of patterns is initially not significantly different. However, the high concentration patterns show a clear tendency of smoothing while the spikiness of low concentration patterns stays constant. This result is robust under changes of the smoothing procedure as well as changes of the length of the measurement window (data not shown).

As a footnote to the mathematically inclined reader it should be pointed out that the diversity of the data (some of the data from the same experimental conditions exhibit clear cyclic and other data more stochastic features) implies that the basic parameters underlying each realization of the time series are probably also influenced by stochasticity. Thus, the fitting of smooth curves serves in this study the purpose of providing a local detrending of the time series with most of the residuals still containing nontrivial correlations. Hence, the calculated spikiness comprises deterministic (e.g., oscillations) and stochastic aspects.

Taken together the above results indicate that CTLs selectively activated to cytotoxicity have signaling patterns that contain more pronounced spikes than the patterns expressed by fully activated CTLs. Furthermore, the spikiness of the signaling patterns associated with selective activation to cytotoxicity stays constant over the first few minutes of signaling. This finding is in stark contrast to signaling patterns associated with full CTL activation, which get smoother over time.

Discussion

This study examines the dual activation threshold of CTLs by a combination of single-cell approaches and numerical analysis of calcium mobilization measurements.

The intriguing feature that cytotoxicity as a function of antigenic stimulus saturates before full CTL activation has been established at the population level by using methods that measure target cell death in parallel with IL release by CTLs (6, 7). However, these approaches have never addressed the question if and how individual CTLs may exhibit two distinct (i.e., dual) activation thresholds: one for target elimination, the other for clonal expansion. Our approach furnishes a steppingstone to answer this challenging question.

Our morphological studies demonstrate that at high antigen concentration a mature IS formed between CTLs and target cells is accompanied by full CTL activation. These data are in good agreement with previous findings obtained for $CD4^+$ and $CD8^+$ T lymphocytes (8, 9, 28). Nevertheless, in our cell system we find that at antigen concentrations inducing solely cytotoxicity the IS is rudimentary, i.e., phosphotyrosine staining and CD2 enrichment at the cell–cell contact site are marginally present or absent. Remarkably, polarization of tubulin cytoskeleton and perforin granules are almost maximal under the same conditions. All in all, our results demonstrate that the orientation of the lytic machinery is a more sensitive response than the formation of a mature IS. They therefore imply that intracellular molecular dynamics allows the definition of two activation thresholds in individual CTLs: one for lytic synapse formation, the other for stimulatory synapse formation.

The observation that the mature IS is not essential for eliciting cytotoxicity is consistent with findings showing that in $CD4^+$ T lymphocytes TCR engagement and signaling are independent of the assembly of a mature IS (12, 13).

The dual activation threshold in individual CTLs can also be observed in FACS analysis experiments in which intracellular perforin contents, a parameter of lethal delivery, are measured.

Comparing TCR down-regulation and IFN-γ production with perforin secretion demonstrates that perforin secretion is easier to trigger than cytokine production. An intriguing observation is that while cytotoxicity saturates at 1 nM of specific peptide concentration, intracellular contents of perforin are decreased by only 40%. This finding is consistent with our observation that in some CTL–target conjugates granule enrichment at the contact site is incomplete while the microtubule organizing center is almost always polarized toward the target (Fig. 2 *Bh*). It is tempting to speculate that only a few lytic granules may be sufficient to kill a target cell (20). This mechanism may play a role in amplifying the efficiency of the cytotoxic response while CTLs save their lytic potential for further encounters with other target cells (10). Our data also show that even though perforin staining decreased with increasing antigen concentrations, this response is saturated when $\approx$80% of total perforin content was lost (Fig. 4*B*). This finding supports the notion that individual CTLs save their lytic potential during cognate interaction with target cells (10).

Also, we characterized the signaling associated with the induction of either only cytotoxicity or full activation. Our analysis indicates that CTLs selectively activated to cytotoxicity have signaling patterns that contain more pronounced spikes than the patterns expressed by fully activated CTLs (Fig. 5). Furthermore, comparing the evolution of signal spikiness induced by high and low antigen concentration shows that signaling properties diverge over time (Fig. 5*F*). That means that the signaling patterns associated with selective activation of cytotoxicity remain spiky, whereas the signaling patterns associated with full CTL activation tend to get significantly smoother over the measurement time.

A visualization of the above results is provided by Movies 1–6, which are published as supporting information on the PNAS web site. In Movies 1–4 the contact of a T cell and a target cell loaded with a high antigen concentration is shown; a clear CTL polarization together with smooth sustained signaling is observed. Movies 5 and 6 show that a low specific antigen concentration suffices to induce CTL polarization accompanied by a spike like signaling.

The above results constitute a characterization of calcium mobilization induced by two different antigen concentrations in CTLs activated to two different effector functions. Our study does not identify a single determinant responsible for different CTL responses. However, our data imply that while the level of calcium signaling is higher with higher antigen dose one additional distinguishing feature may be the spikiness of the signal.

Considering only the average calcium flux we find a considerable overlap between both data sets (Fig. 5*D*). This finding implies that a gene expression dynamics reacting solely to the average calcium flux cannot yield the pronounced differences observed in cytokine secretion. Hence, we suggest that spikiness is in addition to the average calcium mobilization one of the determinants of CTL responses.

The shape determinants of signaling patterns are probably manifold, and current knowledge permits only speculation on the origin of the smooth and spiky signaling patterns found in our study. However, a simple saturation mechanism by which smoothing of signaling patterns is caused by an intrinsic upper limit of calcium mobilization is unlikely to be the principal cause. The reason for this is the progressive decline of spikiness, which is accompanied by a reduction of the mean calcium mobilization in CTLs stimulated by a high antigen concentration (Fig. 5*F*).

In conclusion, we suggest that the synapse structure may also play an important role in shaping intracellular signaling patterns. The two findings that TCR-mediated signaling has at high and low specific peptide concentrations pronouncedly different characteristics and that smoothing of signaling occurs only in the presence of a stimulatory synapse imply that the IS stabilizes the signaling process. Hence, the stimulatory synapse can suppress the influence of stochastic TCR engagement and triggering, thus leading to smooth sustained signaling. TCR-mediated signals may, outside the context of the stimulatory synapse, be more susceptible to nondeterministic influences, such as thermic membrane fluctuations, heterogeneous TCR mobility, and CTL–target cell movement. The influence of such nondeterministic quantities could be reflected by pronounced $[Ca^{2+}]_i$ spikes that are characteristic of TCR signaling at low specific peptide concentration, i.e., signaling in the absence of the stimulatory synapse. Thus, while the lytic synapse orients granules secretion, the stimulatory synapse can provide a stable environment for well defined triggering of TCRs by peptide–MHC complexes, resulting in smooth and sustained signaling.

We thank Oreste Acuto and Denis Hudrisier for meaningful discussion and Pedro Romero and Michal Or-Guil for critical reading and discussion of the manuscript. This work was supported by grants from la Ligue Contre le Cancer "Equipe Labellisee 2001". C.U. was supported by a fellowship (poste vert) of the Institut National de la Santé et de la Recherche Médicale and "Marie Curie Individual Fellowship" Contract HPMF-CT-2002-01541. M.S. and V.C. were supported by Cancer Research UK.

1. Kagi, D., Vignaux, F., Ledermann, B., Burki, K., Depraetere, V., Nagata, S., Hengartner, H. & Golstein, P. (1994) *Science* **265,** 528–530.
2. Lowin, B., Hahne, M., Mattmann, C. & Tschopp, J. (1994) *Nature* **370,** 650–652.
3. Sykulev, Y., Joo, M., Vturina, I., Tsomides, T. J. & Eisen, H. N. (1996) *Immunity* **4,** 565–571.
4. Sanderson, C. J. (1976) *Proc. R. Soc. London Ser. B* **192,** 241–255.
5. Isaaz, S., Baetz, K., Olsen, K., Podack, E. & Griffiths, G. M. (1995) *Eur. J. Immunol.* **25,** 1071–1079.
6. Valitutti, S., Muller, S., Dessing, M. & Lanzavecchia, A. (1996) *J. Exp. Med.* **183,** 1917–1921.
7. Porgador, A., Yewdell, J. W., Deng, Y., Bennink, J. R. & Germain, R. N. (1997) *Immunity* **6,** 715–726.
8. Monks, C. R., Freiberg, B. A., Kupfer, H., Sciaky, N. & Kupfer, A. (1998) *Nature* **395,** 82–86.
9. Grakoui, A., Bromley, S. K., Sumen, C., Davis, M. M., Shaw, A. S., Allen, P. M. & Dustin, M. L. (1999) *Science* **285,** 221–227.
10. Stinchcombe, J. C., Bossi, G., Booth, S. & Griffiths, G. M. (2001) *Immunity* **15,** 751–761.
11. Trautmann, A. & Valitutti, S. (2003) *Curr. Opin. Immunol.* **15,** 249–254.
12. Zaru, R., Cameron, T. O., Stern, L. J., Muller, S. & Valitutti, S. (2002) *J. Immunol.* **168,** 4287–4291.
13. Lee, K. H., Holdorf, A. D., Dustin, M. L., Chan, A. C., Allen, P. M. & Shaw, A. S. (2002) *Science* **295,** 1539–1542.
14. Negulescu, P. A., Shastri, N. & Cahalan, M. D. (1994) *Proc. Natl. Acad. Sci. USA* **91,** 2873–2877.
15. Valitutti, S., Dessing, M., Aktories, K., Gallati, H. & Lanzavecchia, A. (1995) *J. Exp. Med.* **181,** 577–584.
16. Wulfing, C., Rabinowitz, J. D., Beeson, C., Sjaastad, M. D., McConnell, H. M. & Davis, M. M. (1997) *J. Exp. Med.* **185,** 1815–1825.
17. Dolmetsch, R. E., Xu, K. & Lewis, R. S. (1998) *Nature* **392,** 933–936.
18. Takayama, H. & Sitkovsky, M. V. (1987) *J. Exp. Med.* **166,** 725–743.
19. Esser, M. T., Haverstick, D. M., Fuller, C. L., Gullo, C. A. & Braciale, V. L. (1998) *J. Exp. Med.* **187,** 1057–1067.
20. Lyubchenko, T. A., Wurth, G. A. & Zweifach, A. (2001) *Immunity* **15,** 847–859.
21. Kupfer, A. & Singer, S. J. (1989) *Annu. Rev. Immunol.* **7,** 309–337.
22. Puisieux, I., Even, J., Pannetier, C., Jotereau, F., Favrot, M. & Kourilsky, P. (1994) *J. Immunol.* **153,** 2807–2818.
23. Leupin, O., Zaru, R., Laroche, T., Muller, S. & Valitutti, S. (2000) *Curr. Biol.* **10,** 277–280.
24. Hegger, R., Kantz, H. & Schreiber, T. (1999) *Chaos* **9,** 413–419.
25. Berke, G. (1995) *Cell* **81,** 9–12.
26. Burkhardt, J. K., Hester, S., Lapham, C. K. & Argon, Y. (1990) *J. Cell Biol.* **111,** 2327–2340.
27. Blott, E. J. & Griffiths, G. M. (2002) *Nat. Rev. Mol. Cell. Biol.* **3,** 122–131.
28. Potter, T. A., Grebe, K., Freiberg, B. & Kupfer, A. (2001) *Proc. Natl. Acad. Sci. USA* **98,** 12624–12629.